The General Circulation of the Atmosphere

Elizabeth Maroon

May 17, 2009

Abstract

The general circulation of the atmosphere can be divided between two regimes which transport heat poleward, that of the tropics and that of the mid-latitudes and extra-tropics. In the tropics, we see the Hadley Circulation, which on average is the circulation of the tropics. The Walker Circulation of the equatorial Pacific is significant exception. In the mid-latitudes, eddies (synoptic-scale storm systems) move heat poleward. We are able to produce successful analogues of these phenomena with rotating tank experiments by varying the rotation speed of the tank. A low rotation speed (small Coriolis parameter) will produce the laminar over-turning like the Hadley cells, while a high rotation speed (large Coriolis parameter) produces turbulent eddies, as observed in the mid-latitudes.

1 Introduction

We have experimented on many different aspects of the atmosphere over the course of this semester; this final set of tank experiments and synoptic observations is the capstone on all the previous projects. In this project, we examined the general circulation of the atmosphere and observed concepts from previous projects, including thermal wind, convection, and fronts.

The general circulation of Earth's atmosphere is best described by two different zones, those of the tropics and extra-tropics (see Figure 1); both work to transport heat away from the equator, attempting to bring the atmosphere into an equilibrium. In the tropics, angular momentum leads to the creation of Hadley cells where air rises at the equator, travels in the upper atmosphere to a latitude around 30°S/30°N, sinks to the surface, and then returns to the equators. Beyond 30°S/30°N, these orderly cells break down into turbulent eddies (synoptic scale songs) that ultimately transport heat poleward (Illari and Marshall, 2009).

The reason for these differences in is the Coriolis force; the Coriolis parameter,

$$f = 2\Omega sin(\phi), \tag{1}$$

describes the strength of the Coriolis force and is stronger with greater latitude (ϕ). Ω is the rotation of the Earth (7.272×10^{-5} s^{-1}). When the Coriolis parameter is low, organized Hadley cells can form, as seen in the tropics; but where the Coriolis parameter is large, the flow breaks down into turbulent eddies. With tank experiments, there is no variation of latitude, so we can alter the Coriolis parameter by changing the rotation

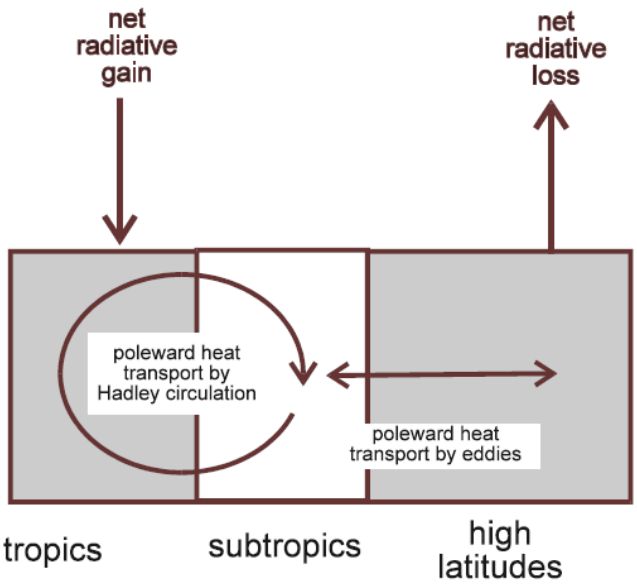

Figure 1: Poleward heat transport in and beyond the tropics. In the tropics, heat is carried from the region of greatest radiative influx by Hadley cells. Once the Coriolis force is too great to allow these orderly cells to continue, the poleward heat transport breaks down into turbulent eddies (synoptic scale storms). Image from Project 4 Description (Illari and Marshall, 2009).

speed. With a low rotation speed we can generate an analog to the tropical Hadley cells, and with a high tank rotation speed, the turbulent eddies of the extra-tropics can be demonstrated (Illari and Marshall, 2009).

2 The Tropics: Meridional Circulations and Trade Winds

2.1 Description of Small Coriolis Parameter Circulations and Relevant Theory

The sun heats the Earth more strongly at the equator than the poles. Heat per unit area is much greater over the tropics than over the poles. If the earth were not rotating, this heat would move over the higher latitudes easily and equalize out the heat distribution easily. However, rotation impedes this motion, setting up the meridional circulations known as Hadley Cells in the tropics (Illari, 2009).

Angular momentum (M) in the Hadley cells is conserved. If most zonal wind (u) is impeded near the surface due to friction, then angular momentum states that once air is free of the boundary layer, we should find greater zonal wind. Angular momentum along a ring of latitude is described by

$$M = \Omega r^2 + ur, \tag{2}$$

where $r = acos(\phi)$. a is the radius of the Earth. If we assume that the greatest heating is at the equator's surface (which isn't a bad assumption in the spring and fall), we

assume $u \approx 0$, so $M = \Omega a^2$. Above the boundary layer, $M = \Omega a^2 cos^2(\phi) + uacos(\phi)$. By conserving angular momentum, we see that $u = 0$. If we move slightly away from the equator(either North or South), we see u intensifying. Observationally, we see these strengthen into subtropical westerly jets around $30°N/S$. The thermal wind relation (Equation 3),

$$\frac{\partial u}{\partial p} = \frac{R}{fp}\frac{\partial T}{\partial y} \tag{3}$$

also states that areas of wind shear should coincide with temperature gradients (T is temperature and p is pressure); as we move from equator to pole, we do indeed see a temperature gradient that intensifies outside of the tropics. Angular momentum states that we should have these Hadley cells continue to the pole where we would find unrealistic infinite velocities. The atmospheric system becomes chaotic and cannot sustain the Hadley circulation after $30°N/S$ where the Coriolis force begins to have a noticeable effect (Marshall and Plumb, 2008).

Angular momentum conservation and a small Coriolis parameter describe most of the features of the Hadley circulation. The region of greatest solar influx (which will also have the greatest sea surface temperature –SST) heats moist air and we observe deep convection. Mass must be conserved: where air is rising, air from both sides of the equator rushes in to take its place. Hence, this is an area where air converges, known as the Intertropical Convergence Zone (ITCZ). In this region of deep (moist) convection, we will find much precipitation and the Earth's rainforests (Plumb, 2009).

The ITCZ will vary slightly with season, because the region that is heated the most by the sun will vary depending on the orientation of the Earth. The latitude of greatest upwelling will shift toward the summer pole. In June, July and August, the ITCZ would be slightly to the north of the equator, and in December, January and February, the ITCZ would be slightly to the south. The Hadley cell that is mostly on the winter-side of the ITCZ is slightly stronger than its counterpart that is further toward the summer side of the ITCZ (Plumb, 2009). This Hadley cell has more latitudes that it can cover before it breaks down in the mid-latitudes.

Once the air has risen above the ITCZ, it reaches the extremely stable tropopause and diverges outward, away from the equator. It continues poleward until the Coriolis force is too large, and the flow breaks down into turbulent eddies. Here, the air subsides, creating a region of high pressure, and very little convection (resulting in little precipitation). Over the land in this region of subsidence, we find the world's deserts. Over the oceans, we find the trade inversion, creating a layer of low level cumulus clouds where moist convection over the ocean ceases where it meets the subsidence (This moist process cannot occur over the dry deserts) (Plumb, 2009).

Zonal winds also vary in the tropics, depending on latitude. With subsidence creating regions of high pressure in the subtropics, and up-welling creating a region of low pressure near the equator. Over the subtropics, the Coriolis parameter is strong enough to create anticyclonic winds. Both of these regions combine to create surface Easterlies in the equatorial regions, known as trade winds. Poleward of the zone of subsidence we see westerlies. The region where the zonal winds change from easterlies to westerlies is a region of little wind, known as the doldrums (Plumb, 2009) (Marshall and Plumb, 2008). See Figure 2 for a visual representation of the origin of the trade winds. Figure 3 gives a full picture of the entire Hadley Circulation.

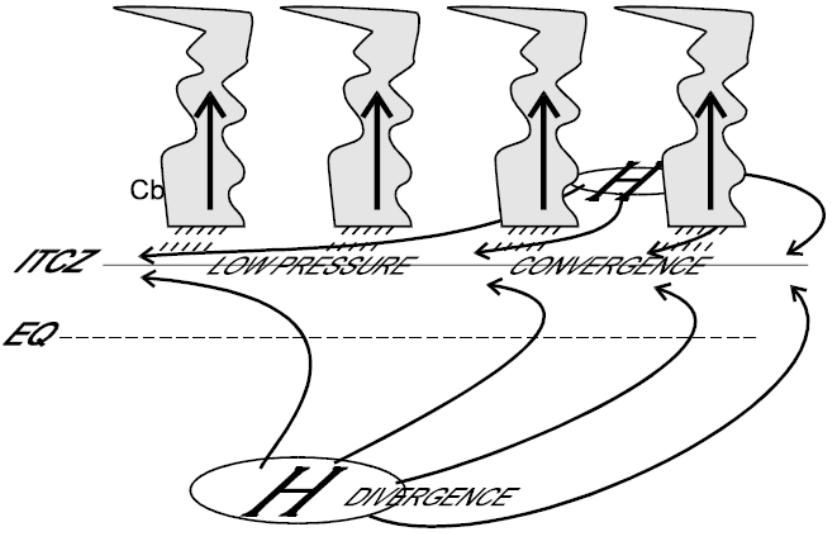

Figure 2: Equatorial easterlies. Divergence from the subtropical regions of high pressure converge at the ITCZ. The Coriolis force creates anticyclonic circulation around these high pressures, resulting in the easterly trade winds along the equator. Image from the 12.333 Notes (Plumb, 2009).

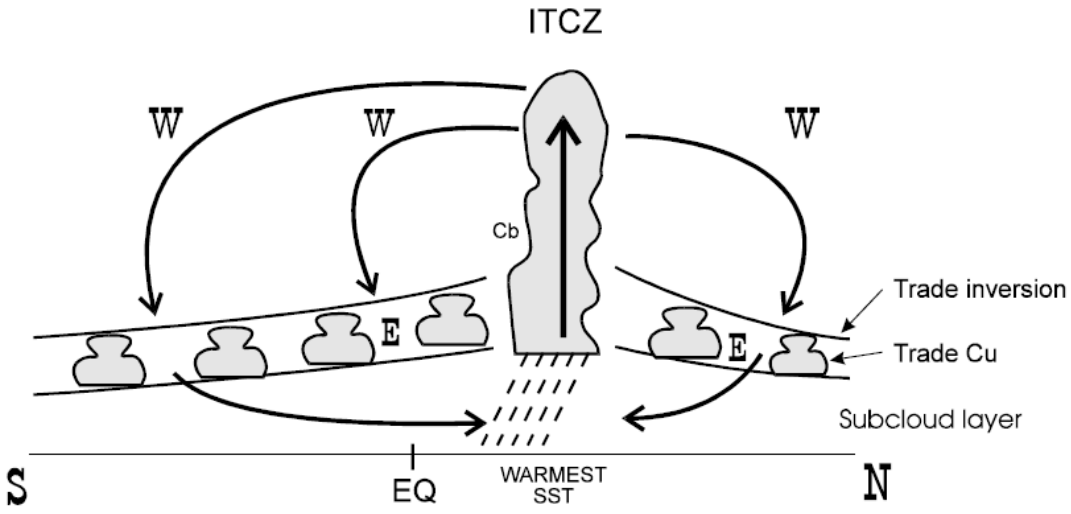

Figure 3: The Hadley Circulation. Hadley cells have deep moist convection extending all the way to the tropopause in the region of highest SST. This now dry air diverges at the tropopause, subsides in the subtropics, and then returns in toward the ITCZ. The regions of great up-welling (ITCZ) produce much precipitation and coincide with the Earth's rainforests. Regions of subsidence, which cannot draw moisture up into the atmosphere, coincide with the world's deserts. The image is from the 12.333 Notes (Plumb, 2009).

2.2 Procedure and Experimental Setup for a General Circulation Rotating-Tank Experiment Analogue

To create a rotating tank analogue that captures these tropical effects, we must first ensure that our Coriolis parameter is as slow as possible. With no latitude variation in the tank, we can only control the rotation rate Ω, which we set as low as possible. In our tank setup, we found that at very low rotation rates, the motor was jerking slightly, which would have introduced turbulence into the experiment. The lowest rotation speed we were able to achieve without this slight jerking was 0.8 rpm. We filled water into the tank (with a height of 20 cm) and placed a smaller tank in the center; this smaller tank would be filled with ice and would represent the 'pole' once the larger tank had reached solid body rotation. Figure 4 shows the experiment setup as it was approaching solid body rotation.

We used three methods to record our observations. The first method was temperature sensors to record the tank's temperature and to help re-confirm the thermal wind relation. Before we filled the tank up, we placed our temperature sensors along one 'longitude.' We used the particle tracking software to determine the azimuthal velocities on the water's surface. The third method was dye and potassium permanganate crystals to illustrate the flow lines in the tank.

After the tank reached solid body rotation, we placed ice in the small tank and gave the system a few seconds so that our Hadley cells could begin. We recorded two trials of particle tracks once the system had reached a steady state. After we were happy with our particle tracking data, we placed permanganate crystals toward the outside of the tank, which would act as our warm equator. As permanganate crystals sink, we hoped that they would capture the easterly flow at our 'equator's' bottom. Dye was placed closer to our smaller ice bucket, which was our analogue to a cool 'pole.'

2.3 Low Tank Rotation Rate Results and Discussion

The data that we gather from all three methods verified our analogue for the tropical Hadley Cell. Our temperature results (see Figure 5) show cold temperatures evolving near the ice bucket 'pole' and warm temperatures at the outside 'equator' of the tank. As the experiment evolved, we see the sensors near the ice bucket decreasing, and eventually other sensors begin to see this cold signal.

Our particle tracking results for two runs of the experiment (see Figure 6). We had a few issues with the particle tracker losing the particles as they moved near our temperature sensors. We did have one particle that made an entire circuit; it spiraled in toward the ice bucket very slightly. We expect this sort of behavior if there is water sinking at the ice bucket. Mass conservation insists that water take the place of the sinking water, and this one track verifies this concept.

We were able to use these particle tracks to find the azimuthal velocities because,

$$v_\theta = r\frac{\partial\theta}{\partial t} \approx r\frac{\Delta\theta}{\Delta t}. \tag{4}$$

From here we processed our particle tracks to find all possible azimuthal velocities (as a function of radius) as seen in Figure 7. For the average azimuthal velocity vs its average radius of each individual track, see Figure 8. We see that at smaller radius, the azimuthal velocity is greater. Thermal wind indicates that over an area of strong

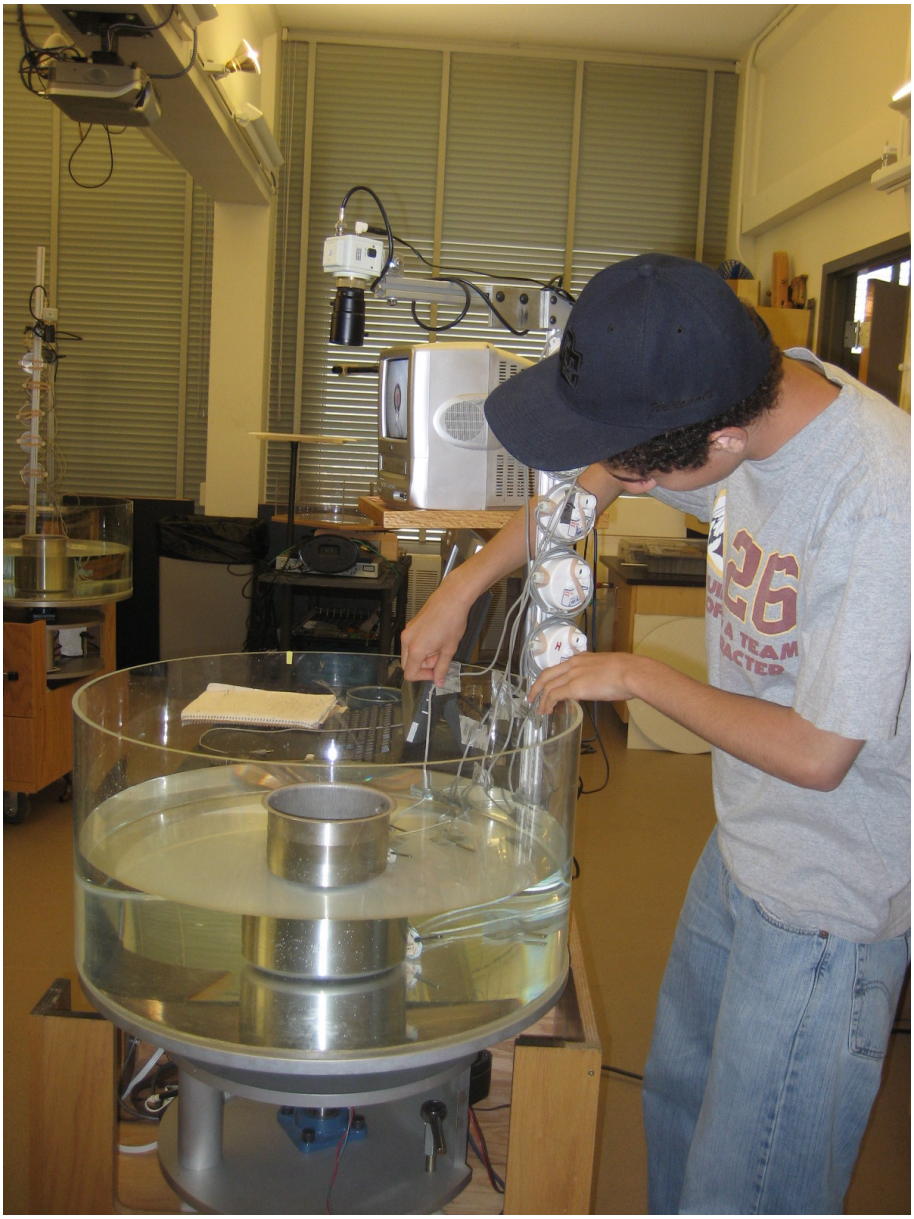

Figure 4: Experiment Setup. Vince examines the temperature sensors on the tank. Temperature sensors are along one 'longitude' so that we can examine one $\partial T/\partial r$ and examine thermal wind balance in that region; we assume that the tank will have azimuthal symmetry and that jets and temperature gradients will be the same at each radius, regardless of 'longitude'.

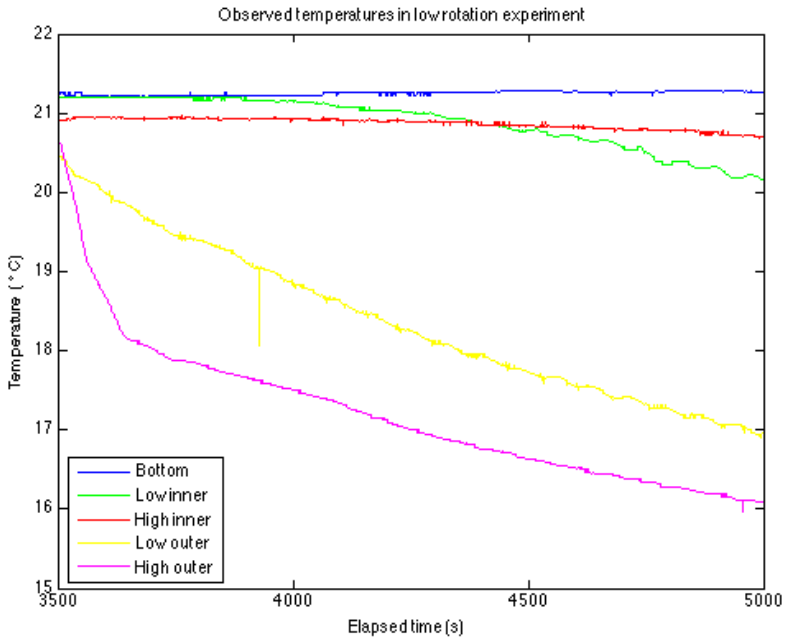

Figure 5: Temperature sensor results over time from the slow rotation experiment. As expected the sensors on the inside of the tank that were nearest the ice bucket 'pole' (purple and yellow) had the quickest drop in temperature. The temperatures at the 'equator,' the outside of the tank (red and blue), stayed at fairly constant warm temperatures. The sensor at the bottom of the tank (green) equally between the ice bucket and edge of the tank cools over time. A temperature gradient is observed between equator and pole.

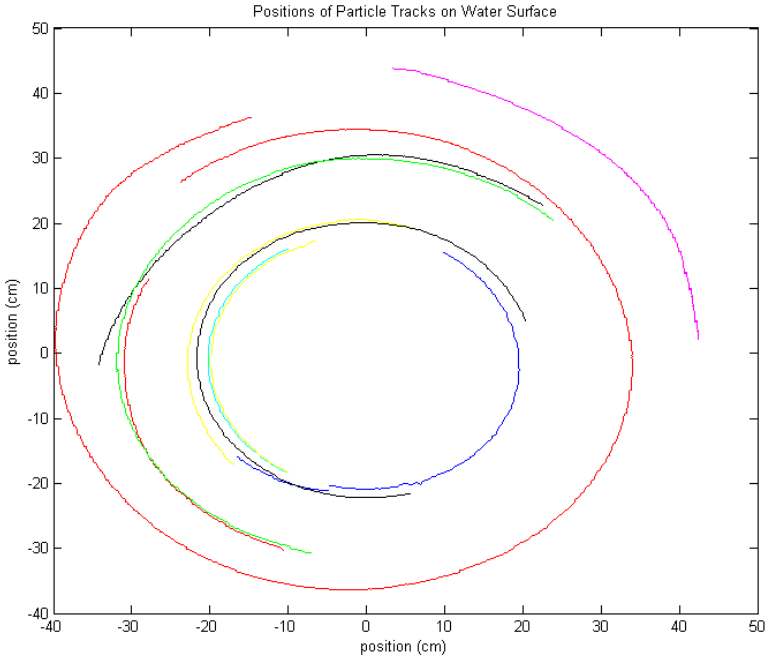

Figure 6: Slow rotation rate tracks. Notice the orderly tracks that the particles follow. There was a little radial inflow as seen by outermost red track that made a complete track around the ice bucket. Subsidence at the ice bucket implies that with sinking water, more water must move into replace it.

temperature gradient, we will find a jet. Our figures visually indicate that the jet has an azimuthal velocity around $1.5 - 1.7$ cm/s.

After determining two linear temperature gradients from our temperature sensor data, we used a discrete form of the thermal wind equation for incompressible fluids,

$$u(r) = -\frac{\alpha g H}{2f}\left(\frac{\Delta T_1}{\Delta r} + \frac{\Delta T_2}{\Delta r}\right) \tag{5}$$

Using data from temperature probes and Equation 5, we calculated that a jet of 1.48 cm/s should be found in our tank. This calculation corresponds well to the jet $(1.5 - 1.7$ cm/s) that we observed. Perhaps it is a bit low because we assumed a linear temperature gradient, which would show us a jet in between the ice bucket and outer edge. We observed the jet closer to the ice bucket, so it is likely that our temperature gradient is also concentrated closer to the ice bucket.

Finally, we were able to visually observe all the features of the Hadley circulation in our tank analogue. The green dye in Figure 9 shows the dye spiral downward and outward along the cold water (that has been cooled by the ice bucket). It shows a vague cone on which the cold water is spiraling downward in a westerly sense. In our tank experiments, westerly means is in the same direction as our tank is rotating, while easterly moves counter to the rotation direction. By defining westerly and easterly in this manner, it allows us to make a stronger, clearer analogy to the Earth's atmospheric circulations. This green cone is our polar front above which we fine the westerly jet that our particle track measured.

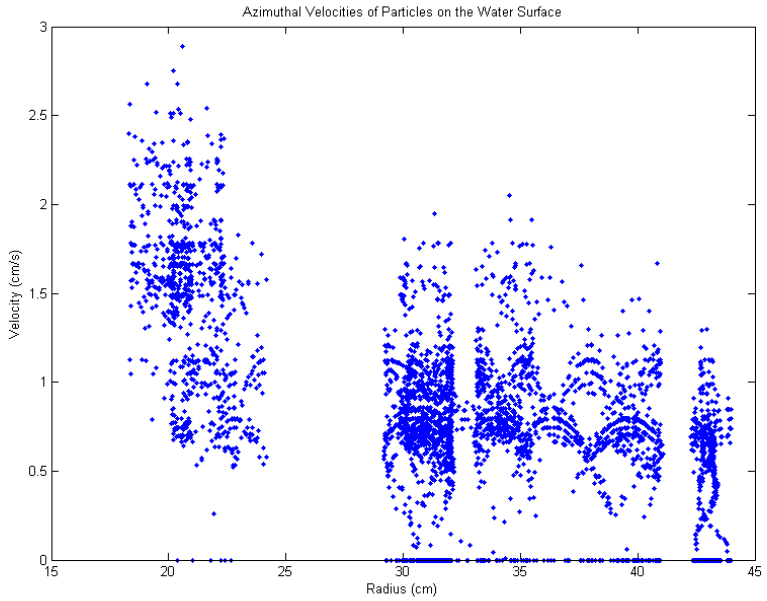

Figure 7: Azimuthal velocities versus radius. All azimuthal velocities between every consecutive particle data point are included, which accounts for the vertical noise. In general, we see greater velocities at the inner part of the tank, which represents that

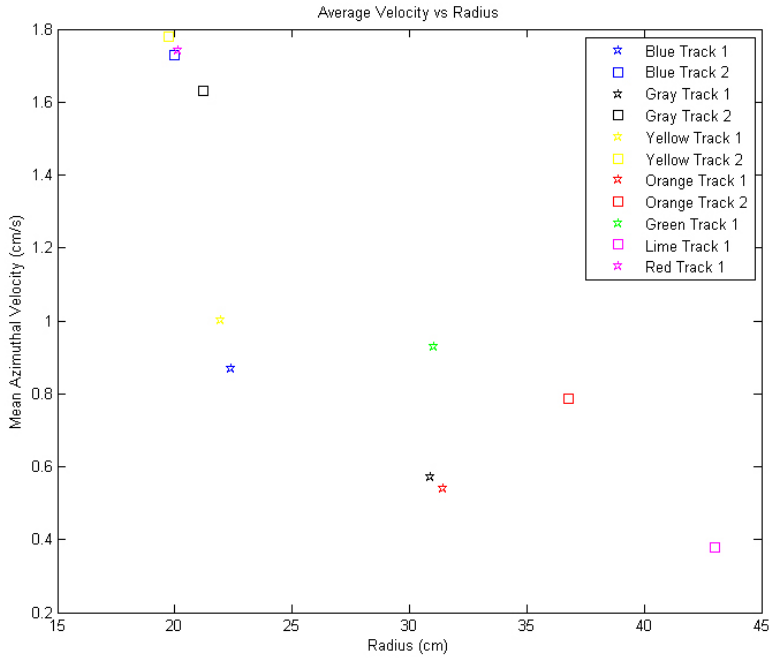

Figure 8: Mean azimuthal velocities for each particle track. Each track's mean azimuthal velocity is plotted against its average radius. This plot allows us to more cleanly see the trend in azimuthal velocities with radius. Again, we see that there is greater velocities with lesser radius. The jet seen at the inner portion of the tank coincides with a temperature gradient between the inner tank and the outer edge.

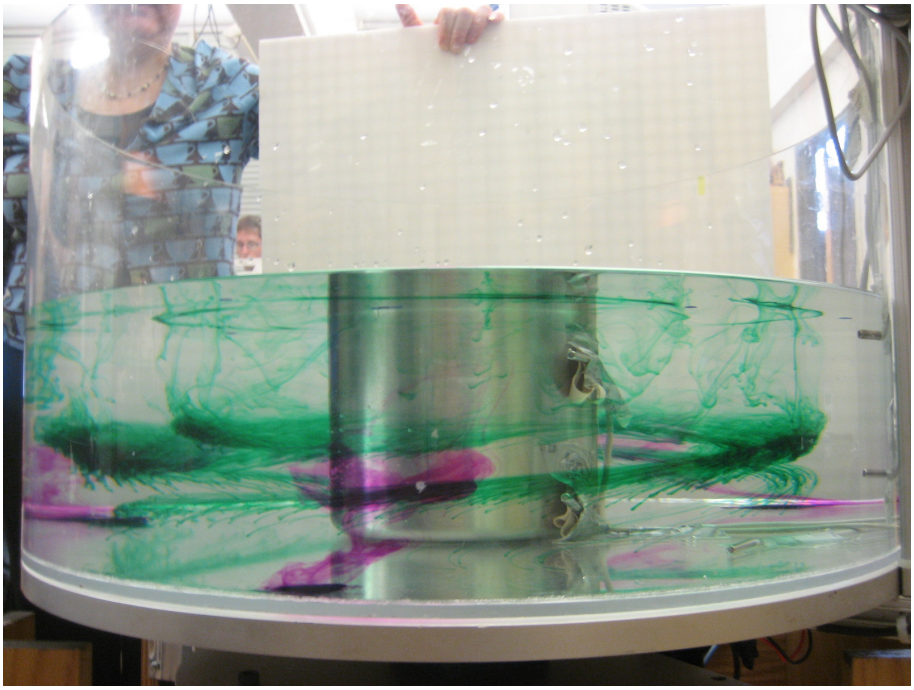

Figure 9: Side view of the low-rotation tank experiment. The green dye spirals downward along the cold sinking water near the ice bucket. It forms a cold cone of water, not unlike our results from our Polar Front Experiment. It is above this green spiral of section that we see our jet.

Figure 10 shows the green dye spiraling outward with the cold water, but it also very clearly shows the purple permanganate. Our tank is rotating counterclockwise, and our permanganate is moving generally clockwise, or easterly. We can clearly see the easterly movement at our analogue for the 'equator.'

Through particle tracks, temperature sensors and dye, our tank shows the following motions:

1. Water sinks near the ice bucket.
2. It reaches the bottom of the tank and diverges outward.
3. Eventually this body of bottom water warms, creating a temperature gradient.
4. This temperature gradient creates a counterclockwise jet at the surface of the tank.
5. The water at the bottom reaches the outer edge of the tank, and is moving slightly clockwise as it rises.
6. To replace the water that downwells at the ice bucket, water at the surface moves inward.

2.4 Observations of Climatology in the Tropics

The same processes we saw in the rotating tank are occurring in the atmosphere, but at a larger scale and with more zonal variation. For the majority of the atmosphere, zonal symmetry is a decent assumption. To better examine the actual Hadley cells in the atmosphere, we examined monthly averages of various atmospheric variations including temperature, potential temperature, zonal wind, meridional wind, and omega. All im-

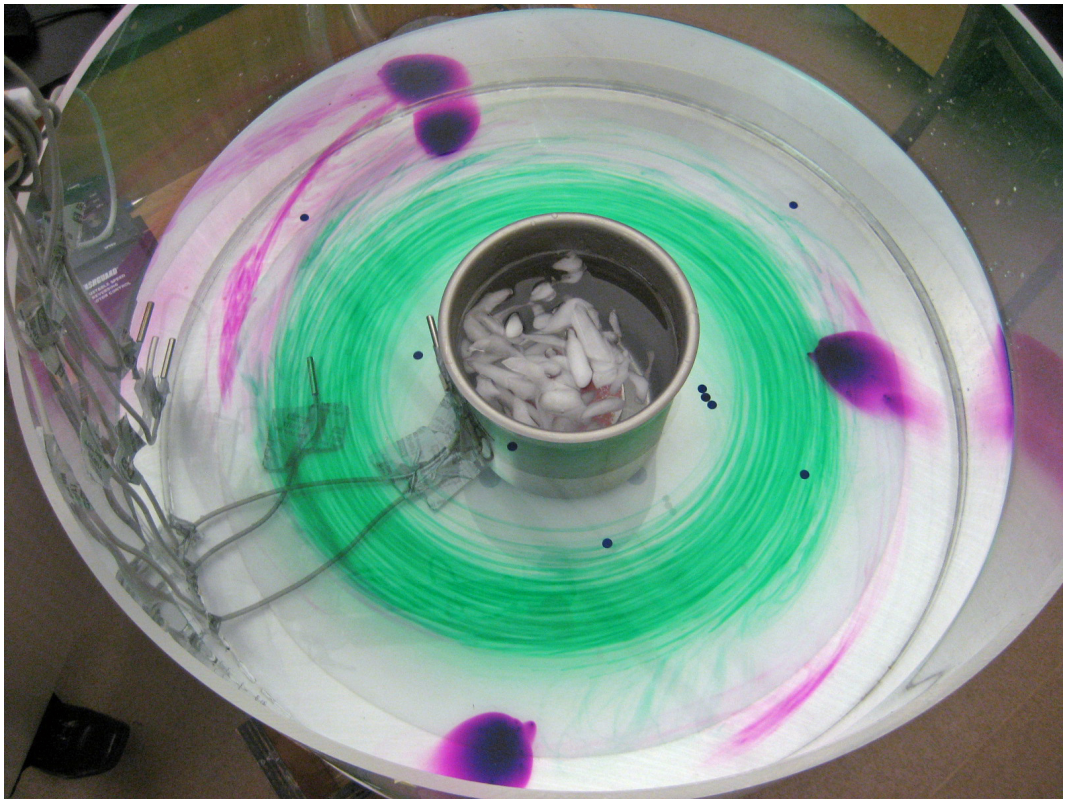

Figure 10: Top view of the low-rotation tank experiment. Here we can more clearly see the potassium permanganate at the outer edges of the experiment. Our tank was rotating counterclockwise. The purple permanganate is drifting outwards and clockwards, or in the analogy of the Hadley cell, as an easterly trade wind.

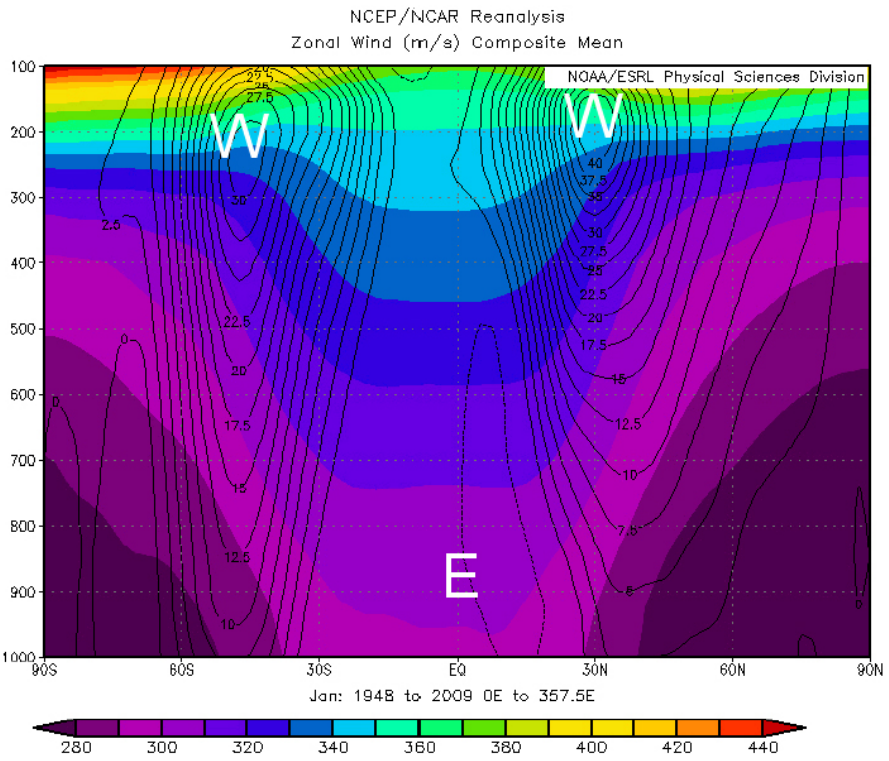

Figure 11: January Mean Potential Temperature and Zonal Winds. Regions of constant potential temperature are marked by the colored contours. Zonals winds are marked by the black contours. Constant potential temperature is horizontal through the tropics, indicating that the region is very well-mixed. Where potential temperature has a strong poleward gradient is also where we find the upper-level westerly jets. Images were produced using NOAA/NCEP data and web interface at http://www.cdc.noaa.gov/cgi-bin/data/composites/printpage.pl.

agery was courtesy of data and a web interface from NCEP (http://www.cdc.noaa.gov/cgi-bin/data/composites/printpage.pl).

Potential Temperature,

$$\theta = T\left(\frac{p_0}{p}\right)^{\kappa}, \tag{6}$$

is a measure for stability in the atmosphere (κ is the ratio of two universal constants, R/c_p). Lines of constant potential temperature are also lines of constant entropy or lines of adiabatic motions. In the tropics we find that the Hadley Circulation mixes the upper and lower atmosphere very well (see Figure 11 for an plot of mean potential temperature and mean zonal wind over many Januaries). Potential temperature is horizontal through the tropics. Beyond the tropics we see potential temperature increase through the mid-latitudes. A potential temperature gradient has the same effect as a temperature gradient, and as expected, and over the steepest gradient is where we see the polar front and the strong upper level westerly jets. In the tropics, we see weak temperature gradients, and the easterlies. The weaker temperature gradients at the surface indicate that the magnitude of easterlies, will be much weaker than the upper-level westerly jets.

Plotting the same data for July shows some important seasonal differences (see Figure 12). The upper-level westerly jets are stronger on the winter hemisphere. We

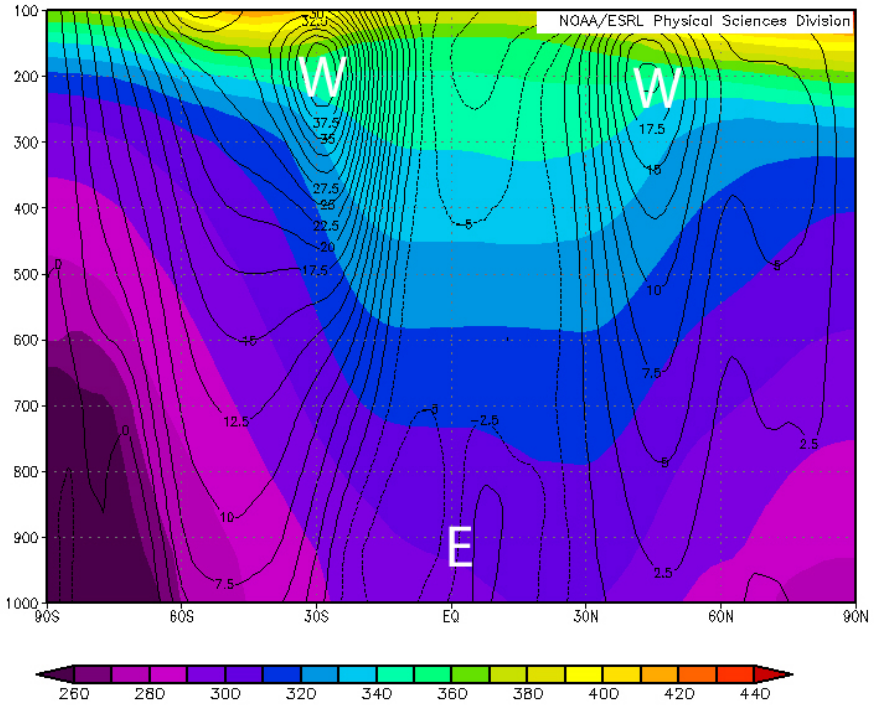

Figure 12: July Mean Potential Temperature and Zonal Winds. When compared to the January means, we see that the stronger upper-level jet is on the winter-side of the equator. Stronger surface easterlies along the ITCZ are seen during July. Image provided by http://www.cdc.noaa.gov/cgi-bin/data/composites/printpage.pl.

also see stronger surface easterlies in July.

The other half of the Hadley Circulation can be examined by using NCEP's interface to plot meridional winds and omega. Omega (ω) is

$$\omega = \frac{Dp}{Dt}, \tag{7}$$

where D/Dt is the total derivative. ω is the velocity of vertical movements in pressure coordinates. Negative ω corresponds to upward motions, while positive ω is downward motion. Figure 13 shows negative ω where we'd expect to see the ITCZ and positive ω near 30°N/S of the equator. The meridional winds and downwelling are stronger in the winter hemisphere. The Hadley circulation is clearly seen with the superimposed arrows. These results are the switched in July when the winter and summer hemisphere switch, but the mechanism is the same.

These mean observations have been zonally-averaged; viewing them without knowing that they are means would imply that the Hadley Circulation appears like this at every longitude. However, this is not the case. The best counter-example is seen along the equatorial tropics (see Figure 14 and 15). The Hadley circulation shows us that along the equator, there should be rising air, but at 130°E, there is sinking air. To the west, air rises, as we expect it to.

These upward and downward motions are connected in a complete circulation by zonal winds (Figure 15). Lower-level easterlies and upper-level westerlies are slightly

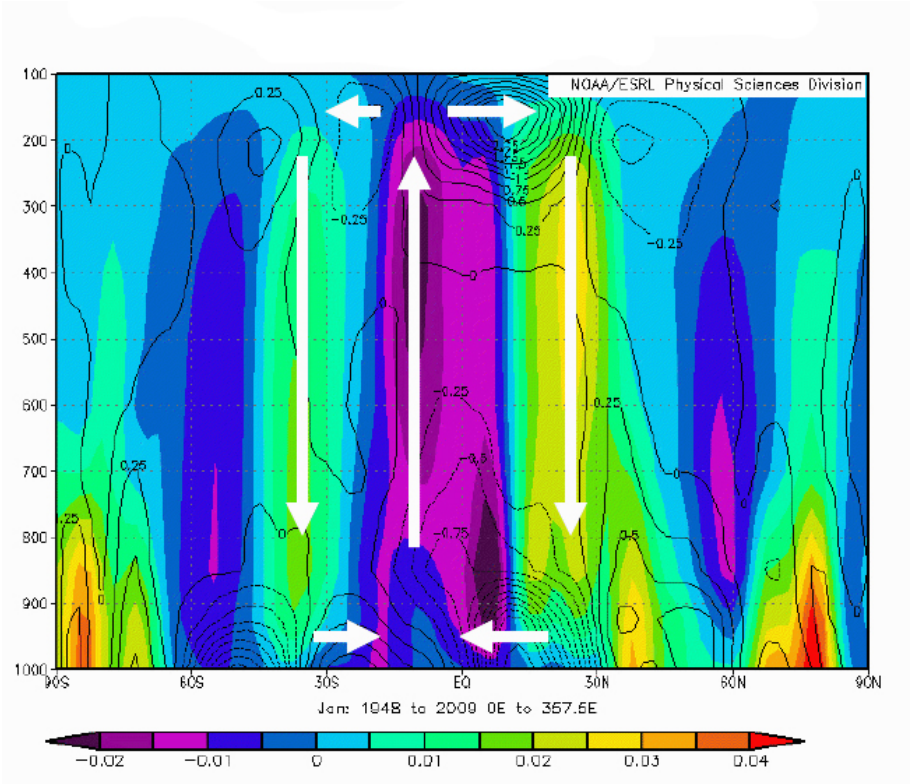

Figure 13: Mean January Meridional and Vertical Motions. Colored contours express the strength of ω, while the black contours show the magnitude of the meridional wind. Arrows are superimposed over the plot to clearly indicate the Hadley cells that have convergence and convection over the region of greatest solar influx and SSTs. Image courtesy of http://www.cdc.noaa.gov/cgi-bin/data/composites/printpage.pl.

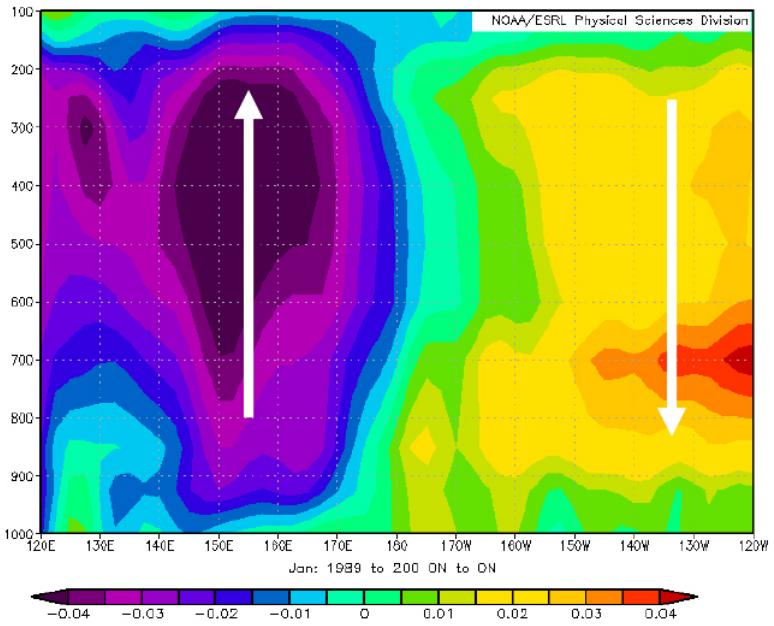

Figure 14: Mean Omega along the Pacific Equator from 1980-present. Color contours represent the mean omega along this cross section of equator from 120°E to 120°W. Air rises to the west of South America and sinks near the maritime continent. Zonal winds connect these two vertical motions to create the Walker Circulation. Assuming that the Hadley Circulation holds at all longitudes is obviously not a completely safe assumption. Image courtesy of http://www.cdc.noaa.gov/cgi-bin/data/composites/printpage.pl.

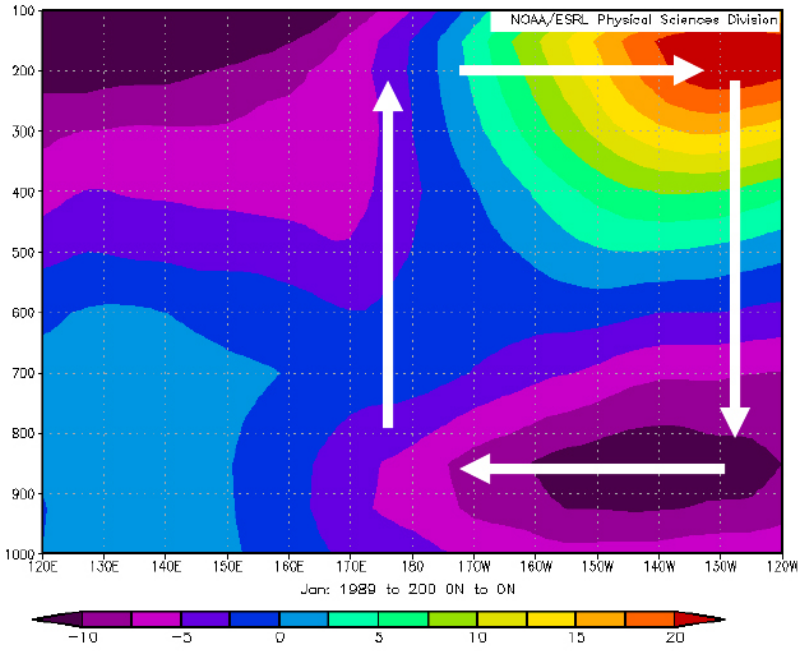

Figure 15: Zonal Omega along the Pacific Equator from 1980-present. Color contours represent the zonal velocities along this cross section of equator from 120°E to 120°W. Omega motions from Figure 12 are represented by the vertical white arrows. The Walker Circulation is this closed circulation in the tropical Pacific. Image courtesy of http://www.cdc.noaa.gov/cgi-bin/data/composites/printpage.pl.

stronger than would be expected by the Hadley Circulation. They complete this important atmospheric pattern known as the Walker Circulation. This circulation is driven by SSTs and coupled atmosphere-ocean circulations. Surface easterlies produce a drag force on the ocean to the west of South America, dragging them westward. To conserve mass, cold water is drawn up to replace it. A cold-water tongue that moves westward is created, further discouraging any deep convection near South America. Near the maritime continent, we find that this cold water has dissipated and that the ocean SSTs are especially warm; deep convection occurs here. Warm air at upper levels has a small westerly velocity that travels back toward South America, completely the circulation. The famous climate variation known as El Niño is caused by slight zonal variations in this circulation that move the regions of convection and subsidence (Plumb, 2009).

3 Beyond the Tropics: Turbulent Eddies and Poleward Heat Flux

3.1 Description of Mid-latitude Circulations and Relevant Theory

In the mid-latitudes and extra-tropics we find that the orderly Hadley circulation has broken down into a series of turbulent eddies. These eddies, or storm systems, are a result of potential energy in the atmosphere in horizontal temperature gradients. The meridional Hadley circulation cannot be organized to release this potential energy. Instead, we find this baroclinic (which means that air density is a function of more than just pressure) instability that creates the eddies and transfers warm air parcels poleward, and cold parcels equator-ward, along 'slantwise convection.' These eddies 'stir' the atmosphere to decrease the temperature differences from equator to pole (Illari and Marshall, 2009).

Overall, we find that the eddies transport heat poleward. The poleward eddy flux due to these eddies is $\overline{v'T'}$, where v' is our meridional velocity variance. The zonal average of this eddy heat flux is $[\overline{v'T'}]$. The net heat flux poleward due to these eddies is

$$H = 2\pi a cos(\phi)\frac{c_p}{g}\int_0^{p_s}[\overline{v'T'}]dp. \tag{8}$$

Here a is the radius of the Earth (6370 km), c_p is the heat capacity at constant pressure (1004 J/K kg), g is 9.81 m/s^2 and p_s is the surface pressure (1000 hPa). Variations of this heat flux equation for our tank experiment and for the atmosphere will illuminate the nature of how heat is transported by eddies.

3.2 Procedure for the High Rotation Case

The procedure for the high-rotation rate case was nearly identical to the low-rotation rate case. The main difference is the greater rotation rate; we used a rotation rate of 8 rpm. We also did not use potassium permanganate to examine our stream flow. Instead we used two different colors of dye (blue and red) to show the swirling eddies.

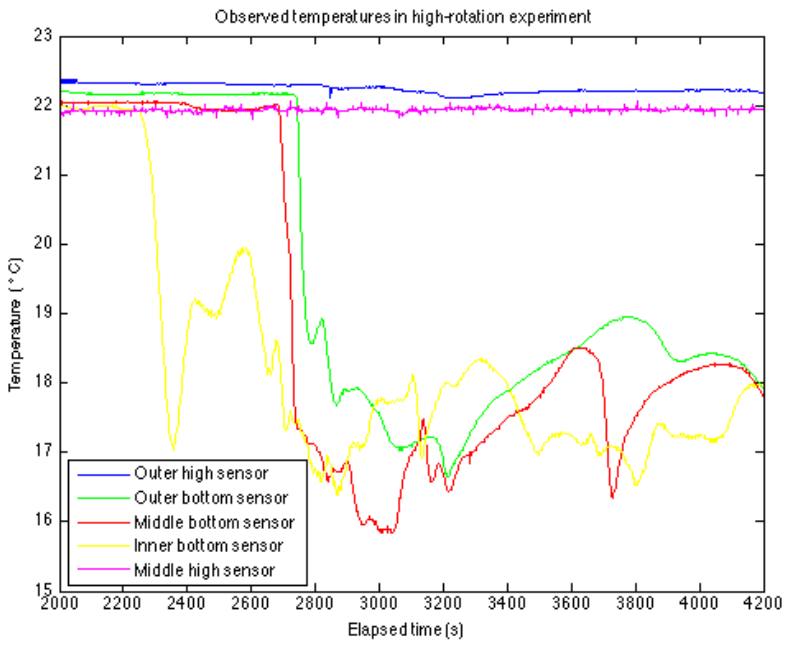

Figure 16: Temperature Probe Results for the High-Rotation Rate Tank Experiment. These temperature sensors had many similarities to those from the low rotation case. The inner and outer top temperature probes (blue and magenta) saw little change in temperature, and only recorded noise, slight temperature fluctuations. The temperature sensors along the bottom (red, green and yellow) recorded the cold water that sunk downward from the ice buckets. This bottom water showed relatively large fluctuations, or eddies.

3.3 High Rotation Rate Results and Discussion

As expected, when we increased the rotation rate in the rotating tank, we found that instead of a gentle overturning, there was large fluctuations of cold and water water along the bottom of the tank (see Figure 16). These fluctuations were part of the eddies. We used these temperature sensors to determine the mean $\overline{T'}$ for the tank.

The particle tracker recorded many swirling tracks from which we can determine the tank's $\overline{v'}$, the mean variance of the radial velocity. Figure 17 shows these tracks.

By adapting Equation 8 slightly, we see that our net heat transfer should be from the melting ice only, such that,

$$L_f \frac{\Delta m}{\Delta t} = 2\pi r \rho c_l \int_0^H [\overline{v'T'}] dz. \tag{9}$$

L_f is the latent heat of fusion of ice, m is the mass of ice in the bucket, t is time it took for the ice to melt, c_l is the heat capacity of liquid water, and H is the height of the water. We have to make a few approximations given that the data from our tank is far from complete. The first assumption is that we use one average r for the tank; we choose the middle of the tank, at about a radius of 36 cm. Our second assumption is that $\overline{v'T'} = \overline{v'T'}$. Because our velocity and temperature variances do not correspond to the same points or times, the best we can do is to average them. Our mean $\overline{v'} = 0.3$ cm/s and the mean $\overline{T'} = 1$ K. With a water height of 20 cm, and a mass of ice around 800 g, we find that the left-hand side of Equation 9 comes to 144 Watts, while the

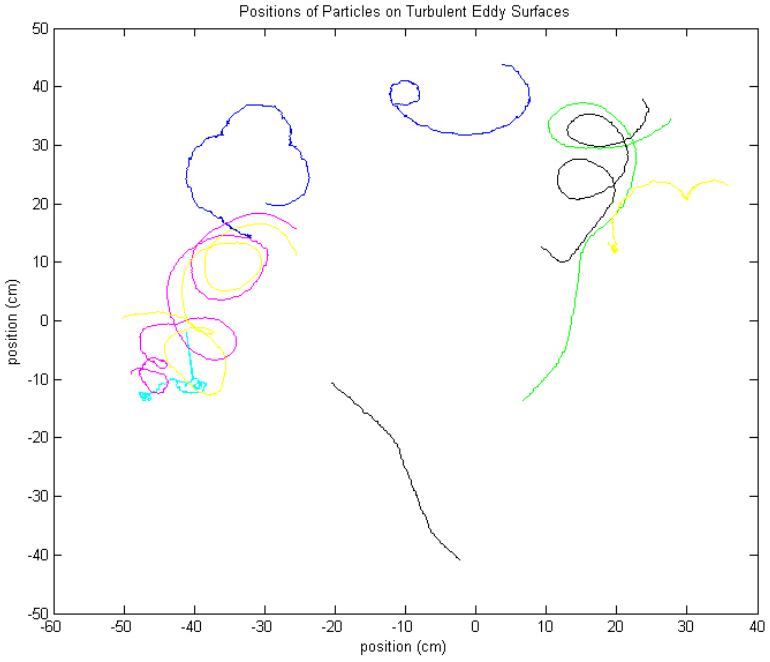

Figure 17: Turbulent Particle Tracks. Note that some particles move in swirling patterns, while others simply move straight out. There was a general trend for particles to move outward from the ice bucket.

right-hand side is an order of magnitude higher at 2380 Watts. The above assumptions are likely the source of error. Given that we've found the largest possible $[\overline{v'T'}]$ by multiplying $\overline{v'T'}$, the right-hand side of Equation 9 should be the upper bound. Given the assumptions in this order-of-magnitude calculation, it is not surprising that the correlation is not exact.

We placed blue dye near the cold water and red dye at the edges to visually see the eddies (see Figure 18). These eddies are vertically coherent, showing only horizontal variations, which is a manifestation of the Taylor-Proudmann Theory.

3.4 Mid-latitudes climatology: Turbulent Eddies and Poleward Heat Flux

After examining the heat flux of the rotating tank experiment, we examined the effects of the eddies in the atmosphere. Using a script provided by Brian Tang (TA extraordinaire), we studied where eddy flux, $\overline{v'T'}$ was strong. Figure 19 shows the vertically averaged $[\overline{v'T'}]$. There are regions where this heat flux is strongest; in the northern hemisphere this around 45°N in the Pacific Ocean and over the western Atlantic Ocean/New England. In the southern hemisphere, we find these fluxes strongest around 45°S, across almost the entire globe. These are regions of cyclogenesis, where mid-latitude storms form, and create the strongest strong heat flux poleward. They are stationary regions over many Januaries, implying that there is some stationary feature that is forcing these patterns; these stationary features are the ocean and the mountain ranges found in these continents. In the southern hemisphere, there is more

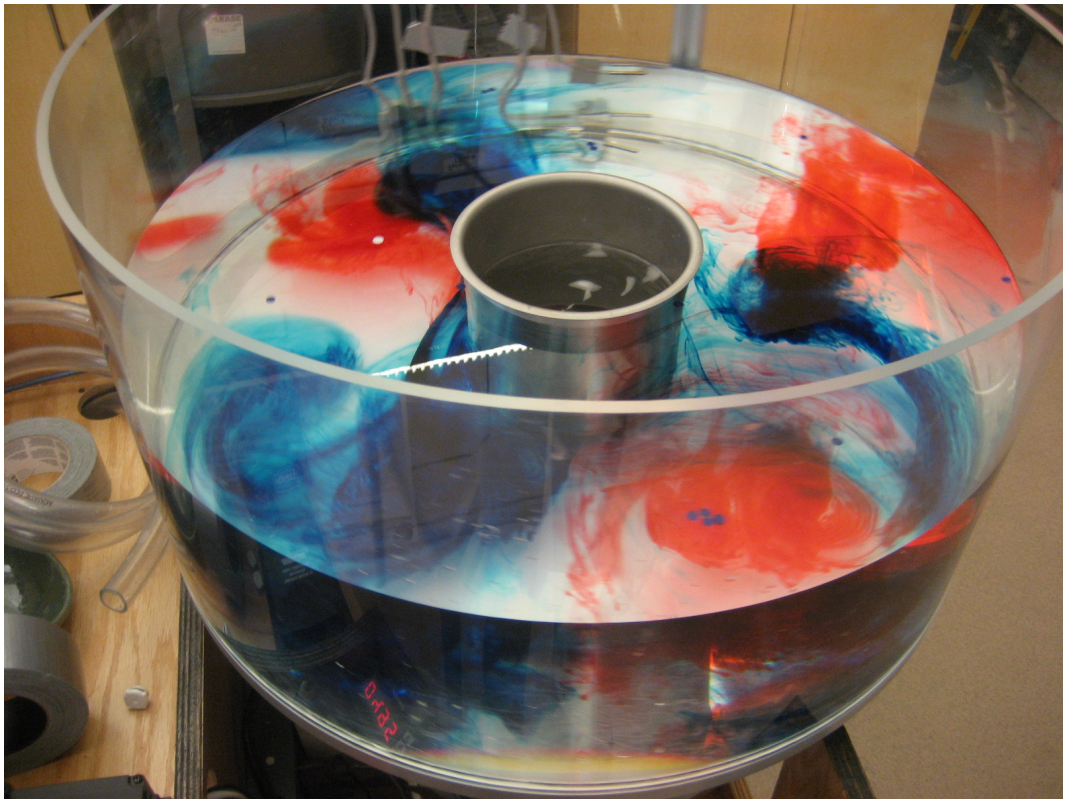

Figure 18: Turbulent Eddies in the High-Rotation Rate Tank Experiment. Some eddies are moving cyclonically about a low (counterclockwise) while others are moving anticyclonically about a high (clockwise). There is vertical 'stiffness' to these eddies; they do not vary vertically, only horizontally, as predicted by the Taylor-Proudmann Theory.

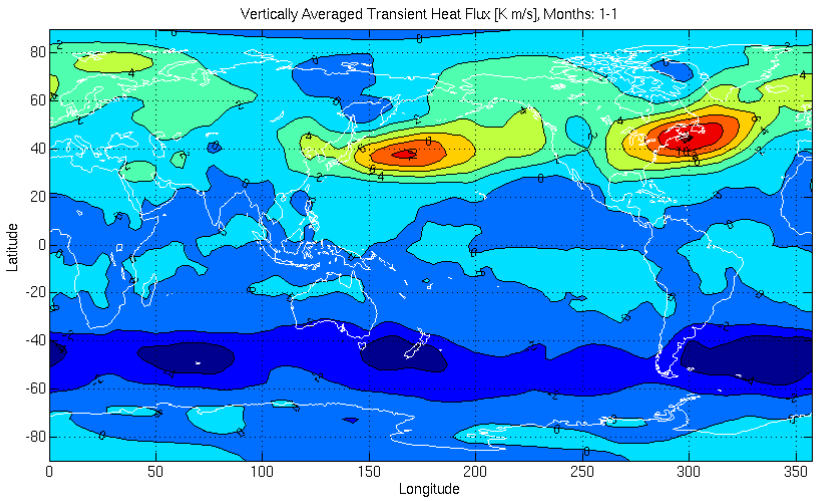

Figure 19: Vertically-Averaged Transient Heat Flux in January. In some regions, there is greater heat flux by turbulent than others. We see this best in regions of storm development over the northern Pacific and eastern North America for the northern hemisphere, and over much of 45°S in the southern hemisphere.

ocean around the entire globe, which explains the more zonally-consistent nature of these tracks.

We examined the poleward heat flux due to the transient eddies in both January and July (see Figure 20). The atmospheric transient eddies transport 1 PW of the total 15 PW that is transported from equator to pole. 1 PW is a significant amount, and should not be ignored. We found that the winter hemisphere has greater heat transport from eddies. Figure 18 shows slightly greater heat flux for the north, but once you consider the southern hemisphere's greater ocean content (which strengthens the eddies), and examine Figure 21, you see that the north's summer eddy flux is signifantly less, but still not negligible. Other sources of heat flux in the atmosphere and ocean are the Hadley circulation and ocean circulations.

4 Connections and Conclusions

Using the rotating tank experiments, we were able to successfully create two analogues to the general circulation of the atmosphere. The first experiment, with a low rotation rate (small Coriolis parameter), showed us the features inherent in the Hadley circulation: an upper-level jet, easterly trade winds, and meridional overturning. With the second experiment at a higher rotation rate (large Coriolis parameter), we examined the heat flux of transient eddies, a suitable analogue to the transient storm systems of the extra-tropics. By examining climatological data, we were able to see that these features, the Hadley Cells and eddies, were transporting heat poleward. A zonal examination of the tropical Pacific revealed the zonal overturning of the Walker Circulation. The existence of the Walker Circulation proved that there is more detail to the general circulation than we have yet studied. But for a first-order examination, the features we have studied explain the majority of the atmosphere's circulation.

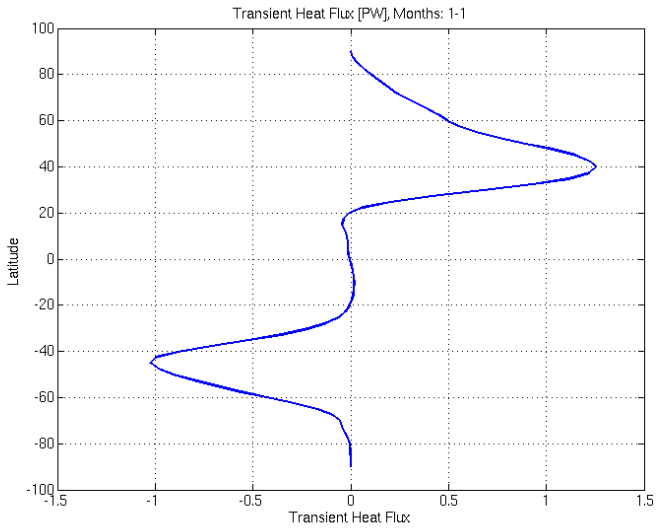

Figure 20: Heat Flux by Transients in January. Transients account for about 1 PW of the 15 total PW heat flux in the atmosphere and ocean. During January, these fluxes are fairly equal in both hemispheres. Transient heat flux is stronger for the winter hemisphere, but the Southern hemisphere's greater ocean content results in nearly equal flux magnitudes for both hemispheres. In July, the flux for the southern hemisphere is almost twice that of the northern hemisphere.

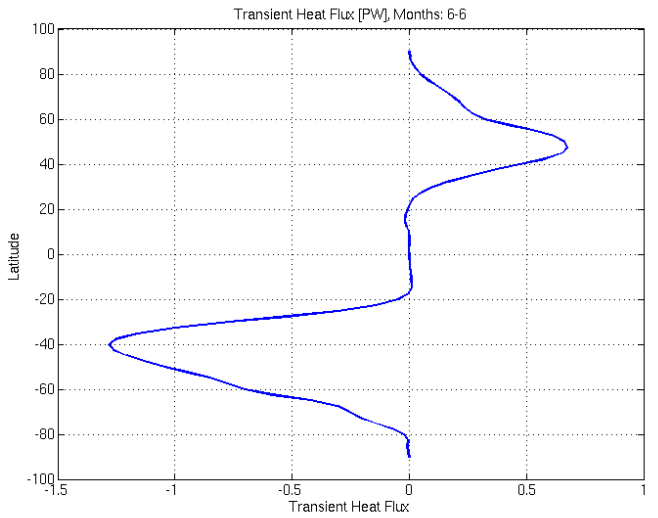

Figure 21: Heat Flux by Transient Eddies in January. During July, the southern hemisphere eddies transports significantly more heat than those of the Northern hemisphere due to its winter season and the greater ocean content.

5 Future Work

A further analysis of the low-rotation thermal wind with more temperature sensors would allow us to see how the temperature gradient varied with space. Although our estimation of the jet from thermal wind was pretty accurate, it is likely that this was by chance. A more accurate description of the temperature gradient would show us more exactly where the jet should be located with reference to the ice bucket.

Further examination of the Walker Circulation would be interesting. Instead of only looking at the climatological Walker Circulation, we should also look at it for individual years and see how its winds and SSTs vary during different phases of the El Niño Southern Oscillation.

References

Lodovica Illari. Weather in a tank: General circulation, 2009. URL http://www-paoc.mit.edu/labguide/circ_hadley.html.

Lodovica Illari and John Marshall. *Project 4: General Circulation*. MIT PAOC, 2009. URL http://www-paoc.mit.edu/12307/gencirc/climatology_lab.pdf.

John Marshall and Alan Plumb. The general circulation of the atmosphere, 2008. URL http://paoc.mit.edu/labweb/notes/chap8.pdf.

Alan Plumb. 12.333 class notes: Chapter 7, 2009. URL http://www-eaps.mit.edu/řap/courses/12333_notes/Chap7.pdf.